Low Energy Defibrillation in Human Cardiac Tissue: A Simulation Study

Stuart W. Morgan,[†] Gernot Plank,[‡] Irina V. Biktasheva,[§] and Vadim N. Biktashev[†*]
[†]Department of Mathematical Sciences and [§]Department of Computer Science, University of Liverpool, Liverpool, United Kingdom; and [‡]Institute of Biophysics, Medical University of Graz, Graz, Austria

ABSTRACT   We aim to assess the effectiveness of feedback-controlled resonant drift pacing as a method for low energy defibrillation. Antitachycardia pacing is the only low energy defibrillation approach to have gained clinical significance, but it is still suboptimal. Low energy defibrillation would avoid adverse side effects associated with high voltage shocks and allow the application of implantable cardioverter defibrillator (ICD) therapy, in cases where such therapy is not tolerated today. We present results of computer simulations of a bidomain model of cardiac tissue with human atrial ionic kinetics. Reentry was initiated and low energy shocks were applied with the same period as the reentry, using feedback to maintain resonance. We demonstrate that such stimulation can move the core of reentrant patterns, in the direction that depends on the location of the electrodes and the time delay in the feedback. Termination of reentry is achieved with shock strength one-order-of-magnitude weaker than in conventional single-shock defibrillation. We conclude that resonant drift pacing can terminate reentry at a fraction of the shock strength currently used for defibrillation and can potentially work where antitachycardia pacing fails, due to the feedback mechanisms. Success depends on a number of details that these numerical simulations have uncovered.

INTRODUCTION

Several clinical trials established that the timely application of an electric shock, particularly with the implantable cardioverter defibrillator (ICD), is the only reliable therapy to prevent sudden cardiac death (1). However, the strong shocks required are reported to have serious adverse effects, most prominently via electroporation, alterations of the action potential waveform and duration (2), depolarization of the resting potential (3), increased pacing thresholds (4), loss of excitability (5), and transient ectopic afterdepolarizations that may initiate postshock arrhythmias (6). Other studies reported mechanical aftereffects such as mechanical dysfunction (stunning), increases in contractility (7), and hemodynamically mediated symptoms (8). Psychological effects on patients play a nonnegligible role (9), and despite long-term survival benefits, patients suffering from arrhythmias that are not immediately life-threatening do not tolerate ICD therapy (10). Biphasic (11), multiphasic (12), and truncated exponential (13) shock waveforms defibrillate at a lower threshold, but still too high for painless defibrillation.

Several approaches to minimize defibrillation energy by employing smarter protocols are under examination, but so far, only antitachycardia pacing has gained clinical significance. Antitachycardia pacing is a series of weak shocks applied at a frequency higher than the intrinsic frequency of the arrhythmia. This therapy has conventionally been applied to slower, presumably hemodynamically tolerated, ventricular tachycardias. Fast ventricular tachycardias (188–250 beats/min) typically receive high amplitude shock therapy, even though antitachycardia pacing may work (14). Although the mechanisms responsible for antitachycardia pacing failure

are not fully understood, an inherent weakness is evident: a fixed pacing frequency is likely to be suboptimal, depending on the arrhythmia. No arrhythmia-specific input is used to form or adjust the antitachycardia-pacing sequence.

In this study we assume that arrhythmias are sustained by reentry and consider a method that employs feedback-driven pacing to control and eliminate the reentry cores, by moving them until they hit inexcitable obstacles or each other, and annihilate. The method relies on a phenomenon of resonant drift (15,16): the drift of reentrant waves when periodic, low-energy shocks are applied in resonance with the period of the reentry. A feedback algorithm (17) is used to maintain the resonance. Resonant drift and its feedback control, herein referred to as resonant drift pacing, have only been studied experimentally in the Belousov-Zhabotinsky reaction medium and in simulations of simplified models of cardiac tissue (e.g., (18–20)).

The goal of this simulation study is to investigate the effectiveness of using resonant drift pacing for low-voltage defibrillation. Previous studies of resonant drift were in models that were very different from modern models of cardiac tissue in many important respects, and their relevance for low-voltage defibrillation is debatable. Here we use an anisotropic bidomain model of cardiac tissue with microscopic heterogeneities and realistic cellular kinetics of human atria. Shocks are applied by injecting current into, and withdrawing from, the extracellular space. Such a description has been used in simulations before, but only to study high-voltage single-shock defibrillation (21).

Our results show that in this model setting, resonant drift pacing can be used to move the core of reentrant activation patterns. Termination can be achieved with high probability, and within the time deemed acceptable by clinicians for antitachycardia pacing to work, at a fraction of the conventional single-shock defibrillation strength, by moving the cores

until they hit an anatomical boundary, or annihilate with each other. We show that in a realistically anisotropic model, direction of movement depends on electrode location and time delays of the shock application, which is in agreement with previous studies (e.g., (15,19)). Knowing the electrode location and the anatomy of the heart, the best delay could be estimated to move the core in the direction of a suitable anatomical structure or boundary (i.e., an inexcitable piece of tissue) that is likely to terminate the reentrant wave.

METHODS

Governing equations

The bidomain model of cardiac tissue is most widely used to study defibrillation-related phenomena (22). The system can be written as

$$C_{\mathrm{m}}\frac{\partial V}{\partial t} = -I_{\mathrm{ion}} + \frac{1}{\beta}\nabla\cdot(\boldsymbol{\sigma}_{\mathrm{i}}\nabla V) + \frac{1}{\beta}\nabla\cdot(\boldsymbol{\sigma}_{\mathrm{i}}\nabla\phi_{\mathrm{e}}), \quad (1)$$

$$\nabla\cdot((\boldsymbol{\sigma}_{\mathrm{i}}+\boldsymbol{\sigma}_{\mathrm{e}})\nabla\phi_{\mathrm{e}}) = -\nabla\cdot(\boldsymbol{\sigma}_{\mathrm{i}}\nabla V) + I_{\mathrm{e}}, \quad (2)$$

where ϕ_{i} and ϕ_{e} are the intracellular and extracellular potential distributions; β is the average cell's surface/volume ratio; C_{m} is the membrane capacitance per unit area; $V = \phi_{\mathrm{i}} - \phi_{\mathrm{e}}$ is the transmembrane potential; $\boldsymbol{\sigma}_{\mathrm{m}}$ and $\boldsymbol{\sigma}_{\mathrm{e}}$ are the intracellular and extracellular conductivity tensors, respectively; I_{e} is the extracellular current; and I_{ion} is the ionic current density through the membrane.

In absence of extracellular current I_{e}, if variations of ϕ_{e} are negligible compared to ϕ_{i}, or if the anisotropy ratios in both domains are the same, Eqs. 1 and 2 can be replaced by a simpler monodomain equation

$$C_{\mathrm{m}}\frac{\partial V}{\partial t} = -I_{\mathrm{ion}} + \frac{1}{\beta}\nabla\cdot(\boldsymbol{\sigma}_{\mathrm{m}}\nabla V), \quad (3)$$

where $\boldsymbol{\sigma}_{\mathrm{m}}$ is the monodomain conductivity tensor.

We used a bidomain description of cardiac tissue, with the exception of monodomain description later than 10 ms after shocks when determining single-shock defibrillation thresholds. A recent comparison of the monodomain and bidomain models suggests that they yield very similar results as long as no strong electric fields are applied (23). To allow comparison with (21), we have used the human atrial model of Courtemanche et al. (24) for the ionic currents, with the alterations described below. This model is well established and very detailed, taking into account all major ionic transport mechanisms and intracellular calcium handling. Note that resonant drift in monodomain models was investigated both with atrial (25) and ventricular (19) cellular kinetics and results were similar, with some difference due to the difference between steadily rotating and meandering spirals. Therefore, we expect that our present result should be interesting for ventricular fibrillation too, subject to a proper account of other important differences between ventricles and atria.

Numerical methods and parameters

All simulations were performed by the Cardiac Arrhythmia Research Package, or CARP (26–28). We used a numerical setup similar to Plank et al. (21). We used a thin sheet of cardiac tissue $4 \times 2 \times 0.02$ cm^3 with the fibers along the x axis, no-flux boundary conditions, and no surrounding bath.

As in Plank et al. (21), the intracellular conductivities in bidomain calculations were fluctuating, with conductivities at different points being uncorrelated random numbers within $\pm 50\%$ of the average,

$$\sigma_{\mathrm{ij}} = \overline{\sigma}_{\mathrm{ij}}(1 + F\eta), \quad (4)$$

where $j = x, y, z$, the level of fluctuations was fixed to $F = 0.5$, and $\eta \in [-1, 1]$ are independent equidistributed random numbers. The justification for intro-

ducing such fluctuations is that although cardiac tissue at a macroscopic scale is frequently approximated as a homogeneous bisyncytium, this is not valid at a microscopic scale, and this makes an essential difference when an external electric field is applied. As the simulation study (21) showed, the presence of fluctuations was fundamental for the mechanism of defibrillation, although the exact value of F was less important. Apart from the $F = 0.5$, which was the maximal considered in Plank et al. (21), we also tried $F = 0.25$ in a few test simulations and found that it was not a principal difference.

Values of the numerous parameters used in this study are presented in Table 1.

Visualization

We used CARP's transmembrane voltage $V(x,y,t)$ output to visualize the results of simulations, using the color-coding shown in Fig. 1 C. The same information was used to detect the wave tips. The wavefront at time t was defined as the line $V(x, y, t) = -23.75$ mV. Then the wave tips for that time were defined as the intersections of the front at time t with the front at time $t - 3$ ms. The time delay of $t = 3$ ms was chosen purely empirically.

To visualize drift, we used a stroboscopic method: we showed positions of the tip synchronized with the signals detected by the registration electrodes.

For meandering spirals this required further refinement, since the stroboscopic selection of tips produced a congested picture, even without any stimulation: so, a five-petal meandering pattern (as shown in Fig. 1 B) produced five clusters of tips. With stimulation, the tip picture becomes even more complicated and unreadable. Therefore, we showed only every

TABLE 1   Details of calculations

| Object/quantity	Notation/value
Bidomain model	$C_{\mathrm{m}}\frac{\partial V}{\partial t} = -I_{\mathrm{ion}} + \frac{1}{\beta}\nabla\cdot(\boldsymbol{\sigma}_{\mathrm{i}}\nabla(V + \phi_{\mathrm{e}}))$, $\nabla\cdot((\boldsymbol{\sigma}_{\mathrm{i}}+\boldsymbol{\sigma}_{\mathrm{e}})\nabla\phi_{e}) = -\nabla\cdot(\boldsymbol{\sigma}_{\mathrm{i}}\nabla V) + I_{\mathrm{e}}$
Monodomain model	$C_{\mathrm{m}}\frac{\partial V}{\partial t} = -I_{\mathrm{ion}} + \frac{1}{\beta}\nabla\cdot(\boldsymbol{\sigma}_{\mathrm{m}}\nabla V)$
Intra- and extracellular potentials	ϕ_{i} and ϕ_{e}
Transmembrane potential	$V = \phi_{\mathrm{i}} - \phi_{\mathrm{e}}$
Transmembrane ionic current density	I_{ion}, as in Courtemanche et al. (24), with alterations
External extracellular current density	$I_{\mathrm{e}}(x, y, z, t)$, by stimulating electrodes
Average cell's surface/volume ratio	$\beta = 1400$ cm^{-1}
Membrane capacitance per unit area	$C_{\mathrm{m}} = 1.0\ \mu$F/cm^2
Extracellular conductivity, tensor	$\boldsymbol{\sigma}_{\mathrm{e}}$
…, along the fibers	$\sigma_{\mathrm{ex}} = 0.625$ S/m
…, across the fibers	$\sigma_{\mathrm{ey}} = \sigma_{\mathrm{ez}} = 0.236$ S/m
Intracellular conductivity, tensor	$\boldsymbol{\sigma}_{\mathrm{i}} = \overline{\sigma}_{\mathrm{i}}(1 + F\eta(x,y,z))$
…, fluctuations intensity	$F = 0.5$
…, uncorrelated equidistributed noise	$\eta(x, y, z) \in [-1, 1]$
…, average, along the fibers	$\overline{\sigma}_{\mathrm{ix}} = 0.174$ S/m
…, average, across the fibers	$\overline{\sigma}_{\mathrm{iy}} = \overline{\sigma}_{\mathrm{iz}} = 0.019$ S/m
Monodomain tissue conductivity, tensor	$\boldsymbol{\sigma}_{\mathrm{m}}$
…, along the fibers	$\sigma_{\mathrm{mx}} = 0.146$ S/m
…, across the fibers	$\sigma_{\mathrm{my}} = \sigma_{\mathrm{mz}} = 0.0182$ S/m
Space discretization step	0.01 cm
Time discretization steps, most of the time	10 μs
…, during and 10 ms after single shocks	1 μs
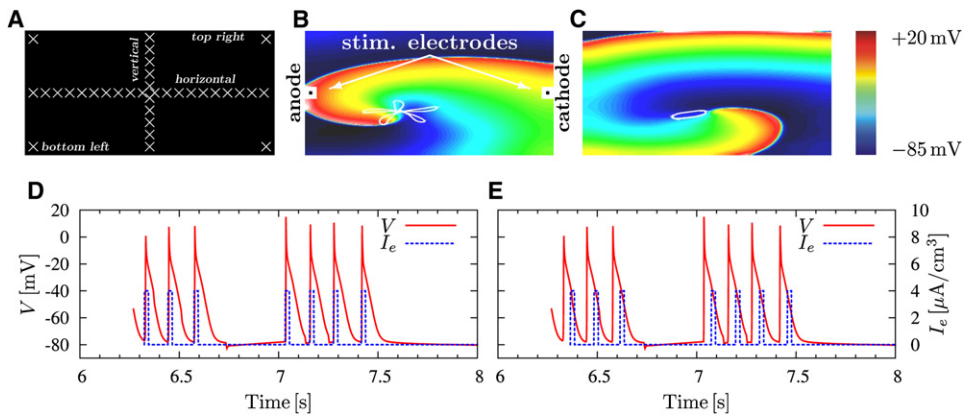
FIGURE 1 (*A*) Locations of registration electrodes. (*B*) Meandering reentry with the trajectory of the tip (*white curve*) and the location of the stimulating electrodes. (*C*) Stationary-rotating reentry with the trajectory of the tip. (*Legend* on the *right*) Color-coding of $V(x, y, t)$. (*D* and *E*) Feedback algorithm with (*D*) $t_{\text{delay}} = 0$ ms and (*E*) $t_{\text{delay}} = 30$ ms. Registered signal (*red solid line*); stimulation shocks (*dashed blue line*), $A = 4 \times 10^6$ μA/cm^3. Intervals between shocks are the same as the reentry periods as registered by the electrode.

N^{th} stroboscopic tip position. Since the meandering patterns were affected by stimulation, we found that the optimal value for N was different from 5; we used $N = 3$.

A possible alternative to the stroboscopic method is sliding averaging of the trajectories. However, it requires careful choice of the averaging window, which may be different in different situations, so we found it less convenient.

Generation of reentry patterns

We used two alterations of the Courtemanche human atrial model (24) of the ionic currents, I_{ion}:

1. To prevent the transmembrane voltages from rising to nonphysiological values during the defibrillation shocks, an electroporation current was included (see (21) and references therein). In addition, a formulation for an acetylcholine-dependent potassium current, $I_{\text{K(ACh)}}$, was added (21,29). This ionic model was used to generate a meandering reentry (see Fig. 1 *B*).
2. In addition to electroporation and $I_{\text{K(ACh)}}$, we used a 65% block of the slow inward L-type Ca^{2+} current coupled with a ninefold increase in the slow delayed outward K$^+$ current and the rapid delayed outward K$^+$ current as suggested by Xie et al. (30). This ionic model was used to generate a stationary rotating reentry (see Fig. 1 *C*).

To initiate reentry, we used an S1-S2 protocol.

Single-shock defibrillation benchmark

Monophasic current shocks $I_e(x, y, z, t)$ were injected into, and withdrawn from, the extracellular space via volumes $0.1 \times 0.1 \times 0.02$ cm^3, stimulating electrodes, centered along the left and right edges of the slab (Fig. 1 *B*). The shocks were of rectangular waveform, 5-ms duration, and varied amplitude A.

Shocks were applied at 12 different timings t_0, separated by 10-ms intervals, after the same initial conditions. This covered an entire single rotor cycle, 120 ms. A single shock was deemed successful if no reentry was detectable at 500 ms after its end. We define the single-shock success threshold as the shock amplitude giving a 50% success rate across the 12 timings.

Resonant drift pacing

Repetitive low-amplitude shocks, of the same waveform and via the same stimulating electrodes as above, were applied at the time moments determined by signals received via registration electrodes.

Six different locations for the registration electrodes were used: point electrodes $0.02 \times 0.02 \times 0.02$ cm^3 in the top-left, top-right, bottom-left, and bottom-right corners; and line electrodes (18) (of cross-section 0.02×0.02 cm^2) through the whole medium, either horizontally, along the fibers, or vertically, across the fibers (see Fig. 1 *A*).

The signal from a registration electrode was defined as the average potential at all the nodes covered by it. The signal triggered a shock application when it exceeded −55 mV. A shock was applied with a delay t_{delay} after it had been triggered. In most cases, we set $t_{\text{delay}} = 0$ (see Fig. 1 *D*). To demonstrate its effect on the direction of the drift, we set $t_{\text{delay}} = 30$ ms, approximately one-quarter of the reentry period (see Fig. 1 *E*).

In all simulations, the registration electrodes were deactivated for a blanking time, $t_{\text{blank}} = 50$ ms, after a shock application.

For the meandering reentry, resonant drift pacing was considered successful if the reentry was terminated sooner than the self-termination time of the reentry, 16,000 ms. For the stationary rotating reentry, this time was extended to 30,000 ms.

RESULTS

Single-shock defibrillation results

We have varied the timings, and strength A, of the single shocks to assess the variability of the outcomes. Consistent with previous observations (21), there were three typical single-shock defibrillation outcomes for both the meandering and stationary-rotating patterns:

1. Strong enough shocks annihilated reentry immediately (Fig. 2 *A*).
2. Weaker shocks led to multiple wavebreaks (Fig. 2 *B*).
3. Weaker still shocks only shift reentry in space (Fig. 2 *C*).

We have found the single-shock defibrillation threshold to be $A = 14 \times 10^6$ μA/cm^3 for the meandering patterns and 18×10^6 μA/cm^3 for the stationary-rotating patterns (Fig. 2 *D*).

Resonant drift pacing results

We tested resonant drift pacing on the meandering, and stationary rotating, reentrant patterns with shock amplitudes lower than the corresponding single-shock defibrillation success thresholds.

Meandering reentry

Point registration electrodes

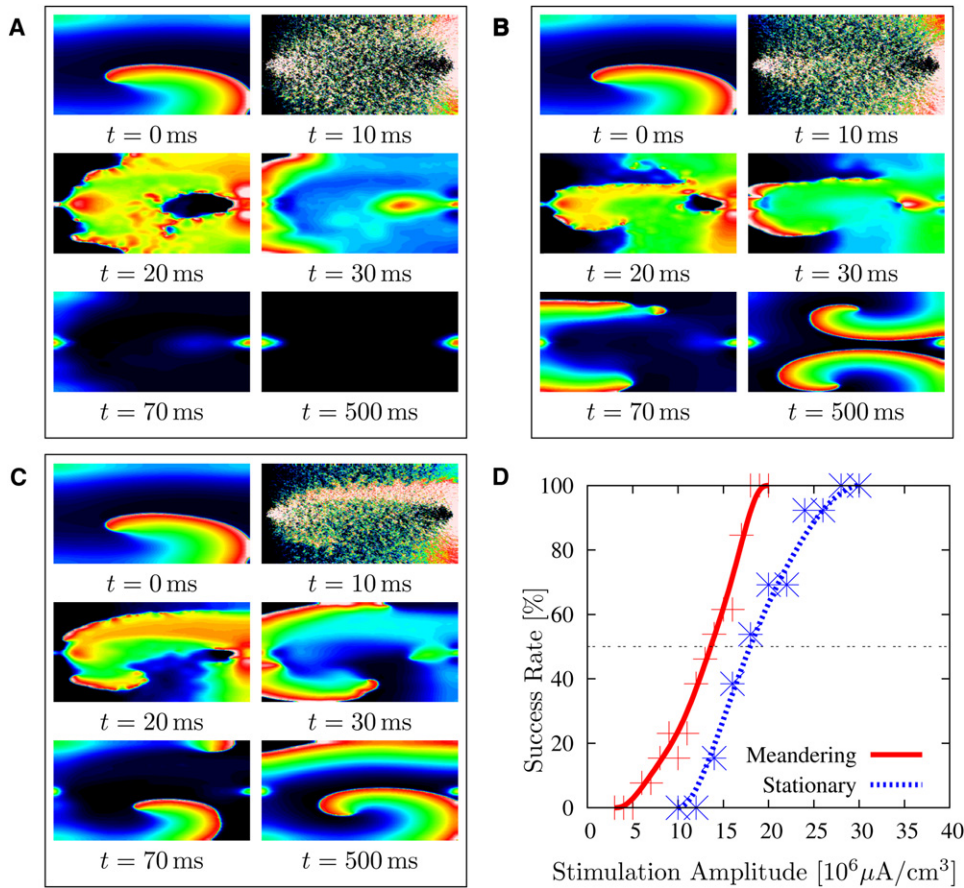Depending on the shock strength, the following outcomes were observed:

FIGURE 2 Single-shock defibrillation, stationary rotating reentry. (*A*) Termination, $A = 16 \times 10^6$ μA/cm^3 applied at $t = 10$. (*B*) Breakup, $A = 14 \times 10^6$ μA/cm^3 applied at $t = 10$. (*C*) Displacement, $A = 12 \times 10^6$ μA/cm^3 applied at $t = 10$. (*D*) Percentage of successful terminations as function of shock amplitude *A*. (*Markers*, raw data; *lines*, Bezier approximation.)

The original reentry drifted, roughly toward the registration electrode, until termination on an inexcitable boundary (see Fig. 3 *A*).

Secondary reentrant patterns were generated near stimulating electrodes; both the original and newly generated reentries drifted. (An example is shown in Fig. 3 *B*.) The original reentry *A* was terminated by the first 24 shocks. However, a secondary reentrant pattern *C* was generated by a shock in the process. After *A* terminated, it was *C* that triggered the subsequent shocks. A third

reentrant pattern, *B*, was generated by a further shock. Due to the proximity of pattern *B* to the registration electrode, it took over the control of the shock applications. Reentry *B* drifted to the boundary and terminated after a further 15 shocks. Then *C* was again the solitary reentry and took over the control. A fourth reentry, *D*, was generated by a shock and, due to its proximity to the registration electrode, took over the control. After three shocks, *D* collided with *C* and they annihilated each other without reaching an inexcitable boundary.
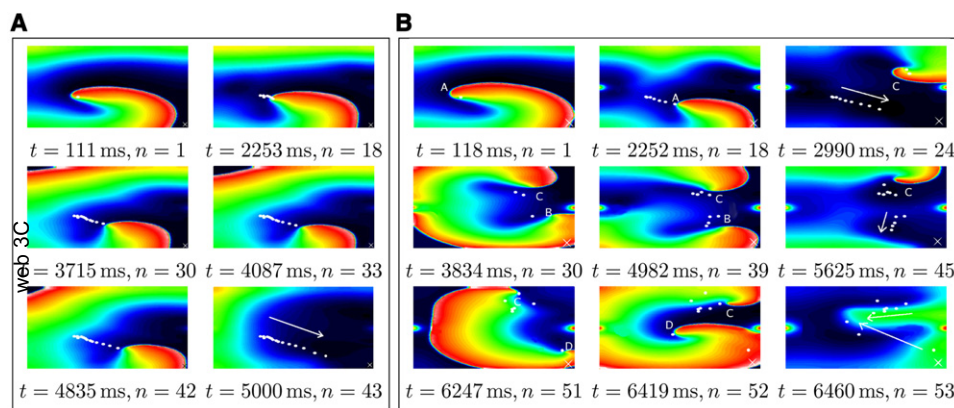

FIGURE 3 Resonant drift pacing of a meandering reentry. (*A*) $A = 1 \times 10^6$ μA/cm^3, reentry drifts to the boundary and terminates. (Here and below, *cross*, location of the registration electrode; "$n = ...$" is the number of shocks applied so far; *open dots*, positions of the spiral tip at every third registered period. (*B*) $A = 2 \times 10^6$ μA/cm^3, original reentry *A* drifts to the boundary and terminates. Additional reentrant patterns *B*, *C*, and *D* are generated by the shocks and trigger further shocks themselves. Pattern *B* terminates at the boundary; patterns *C* and *D* annihilate each other. (*NB*, resonant drift pacing handles multiple patterns.)
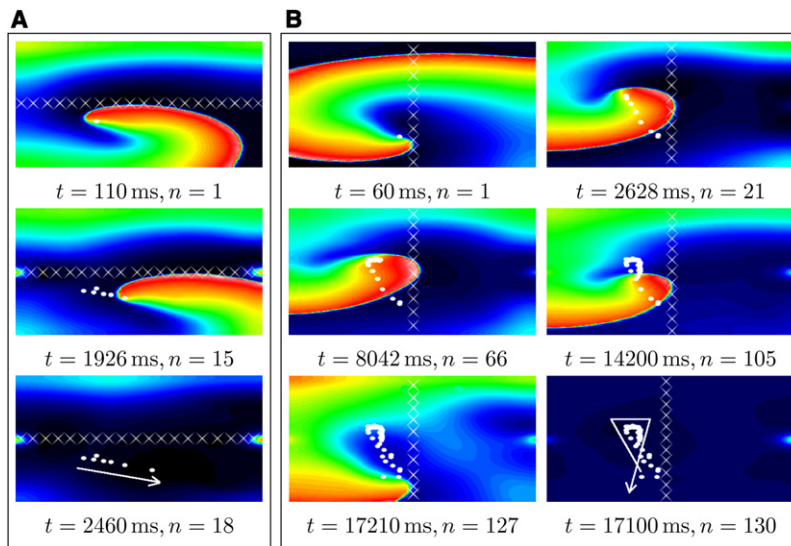
FIGURE 4 Resonant drift pacing with line registering electrodes. (*A*) Horizontal electrode along the fibers, $A = 2 \times 10^6$ μA/cm^3. The reentry drifts resonantly at an angle to the electrode, reaches the boundary, and terminates. (*B*) Vertical electrode across the fibers, $A = 1 \times 10^6$ μA/cm^3. The reentry drifts upwards for 21 shocks, then changes direction and reaches the boundary after a further 109 shocks.

Note that mutual annihilation of reentrant patterns in the bulk of the tissue could be a plausible explanation as to why Pak et al. (31) saw no evidence of annihilation at the ventricular boundaries when testing a protocol similar to the resonant drift pacing.

Line registration electrodes

Horizontal electrode: With the registration electrode along the fibers, the reentry drifted at a small angle to it (Fig. 4 *A*).

Vertical electrode: With the registration electrode across the fibers, the drift was usually more complicated. An example is shown in Fig. 4 *B*. The reentry initially drifts upwards along the electrode. After 21 shocks, the drift turns downwards, until it reaches an inexcitable boundary after a further 109 shocks and terminates. The trajectory of the drift crosses itself, which is not allowed in the asymptotic theory of drift of rigidly rotating spiral waves (17) and was not observed in

our simulations of a stationary rotating reentry, so we consider it a new feature due to meander.

The time taken for termination of all reentrant activity using different locations of the registration electrode is shown in Fig. 5 *A*. It shows that resonant drift pacing can successfully terminate meandering reentrant patterns using shocks 14-times weaker than the single-shock defibrillation threshold. Termination was achieved in all simulations in this series.

Among the registration electrodes, the vertical line was the most successful, as it produced the largest proportion of successful terminations in the fastest time except at the smallest amplitudes. Using a point-electrode in the top right location was the least successful.

We conclude that the termination time depends on the mutual position of the registration electrode, anode, cathode, initial position of the reentry, tissue size, and fiber orientation.

For amplitude $A = 1 \times 10^6$ μA/cm^3, reentry termination time for the meandering pattern, in most cases, was longer

A	Bottom left	Bottom right	Top left	Top right	Vertical line	Horizontal line
1	19169	5013	16763	10239	17600	9510
2	1297	6478	4880	9712	3530	2440
3	5930	2689	6474	4960	580	3180
4	9820	3530	4160	2310	480	7290
5	2060	560	2160	2670	470	3300
6	2570	560	1100	1730	770	810
7	900	920	1300	3590	450	560
8	1660	340	720	1330	260	560
9	460	1290	750	4385	250	460
10	230	330	1230	3820	150	340

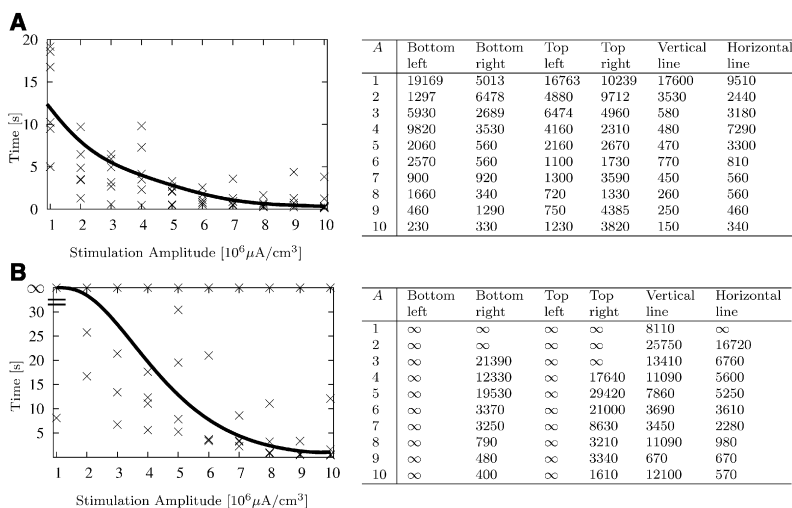| A	Bottom left	Bottom right	Top left	Top right	Vertical line	Horizontal line
1	∞	∞	∞	∞	8110	∞
2	∞	∞	∞	∞	25750	16720
3	∞	21390	∞	∞	13410	6760
4	∞	12330	∞	17640	11090	5600
5	∞	19530	∞	29420	7860	5250
6	∞	3370	∞	21000	3690	3610
7	∞	3250	∞	8630	3450	2280
8	∞	790	∞	3210	11090	980
9	∞	480	∞	3340	670	670
10	∞	400	∞	1610	12100	570

FIGURE 5 Resonant drift pacing results. (*A*) Meandering reentry. (*Left*) Termination time as a function of shock amplitude *A* (*smooth curve*), Bezier approximation. (*Right*) The raw data, time in milliseconds, and amplitude *A* in 10^6 μA/cm^3. (*B*) Same as for panel *A*, but for a stationary rotating reentry; ∞, infinite loop.

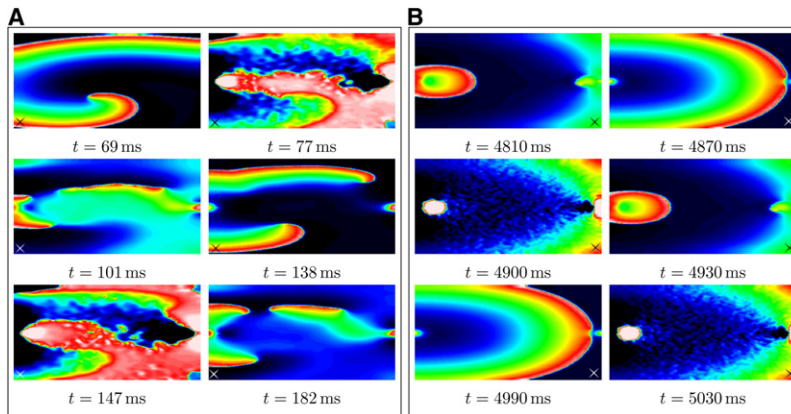FIGURE 6 Infinite loops in resonant drift pacing. (*A*) $A = 10 \times 10^6 \, \mu\text{A/cm}^3$. New waves with breaks are initiated by shocks and trigger further shocks. (*B*) $A = 2 \times 10^6 \, \mu\text{A/cm}^3$. New waves without breaks are initiated by shocks and trigger further shocks.

than its self-termination time of 16,000 ms. Thus, we did not consider lower values for the stimulation amplitudes.

Stationary rotating reentry

Fig. 5 *B* shows the times taken for annihilation of all reentrant waves for the different locations of the registration electrode. Resonant drift pacing can terminate stationary-rotating patterns using amplitudes 18-times lower than the single-shock threshold. The combination of shock strength with the location of the registration electrode affects the probability of success and the time taken for termination.

Termination of stationary rotating reentry was not always observed within the 30,000 ms limit. Sometimes the algorithm gets caught in an infinite loop (Fig. 6), when the original reentrant pattern has been terminated, but shocks produce new wavefronts that trigger further stimulation producing further wavefronts, and so on.

Direction of drift

The theory of the resonant drift (15) predicts that the drift direction depends on the stimulation phase. This dependence leads to the relationship between the drift direction and the delay in the case of a feedback controlled forcing (17,32). A delay by a certain fraction of a spiral's period causes a change in the drift direction by the same fraction of 360°. We have verified that it works in this realistically anisotropic bidomain model as well.

Fig. 7 *A* shows fragments of two such simulations, with the same initial conditions and different values of t_{delay}, 0 and 30 ms, which is approximately one-quarter of the reentry period. The direction of the drift in these two cases differs roughly by ~90°, with account of the anisotropy, in agreement with Biktashev and Holden (17,32).

Using a time delay to induce success

We have mentioned in a previous section that resonant drift pacing may fail through an infinite loop of wavefront eliminations and creations. If newly created wavefronts are unbroken (as in Fig. 6 *B*), then the reentrant activity will

vanish if the stimulation is stopped at any time—i.e., resonant drift pacing will succeed.

A genuine failure occurs when newly created waves are broken and form new reentries (as in Fig. 6 *A*). The chances of getting in such a loop depend on the drift trajectory, which depends on the location of the registration and stimulation electrodes and the feedback delay. Hence, such loops should be avoidable by an appropriate choice of the electrode locations and/or of t_{delay}. In a real-life situation, such a choice would require a great deal of information and could be difficult to make. Not all theoretical solutions (e.g., optimal positions of the electrodes) are necessarily possible to implement in practice. Further, the optimal parameters may vary from one arrhythmia episode to another, so it is difficult to predict a priori.

Of all the mentioned parameters, t_{delay} is the easiest to change, and it may even be adjusted in real time, during pacing. Hence, we propose that a change of the feedback delay could be used to discontinue an infinite loop even after it has already started.

Fig. 7 *D* illustrates the feasibility of this approach. It is a rerun of the simulation of Fig. 6 *A*, with t_{delay} increased to 30 ms at $t = 1000$ ms. This broke the loop and terminated the reentry.

DISCUSSION

Summary of results: resonant drift pacing works in a realistic model of electric field action on cardiac tissue

This simulation study presents results that can be used as experimentally testable hypotheses. It has been based on the understanding of the mechanism by which external electric current affects excitation and propagation via nonuniformity of the electric field and the heterogeneity of the tissue conductivities. This mechanism implies both a strong action near electrodes due to the electric field inhomogeneity, and a weaker, but far-reaching action in the bulk of the tissue due to omnipresent tissue heterogeneities. This model has been used before to simulate single-shock defibrillation
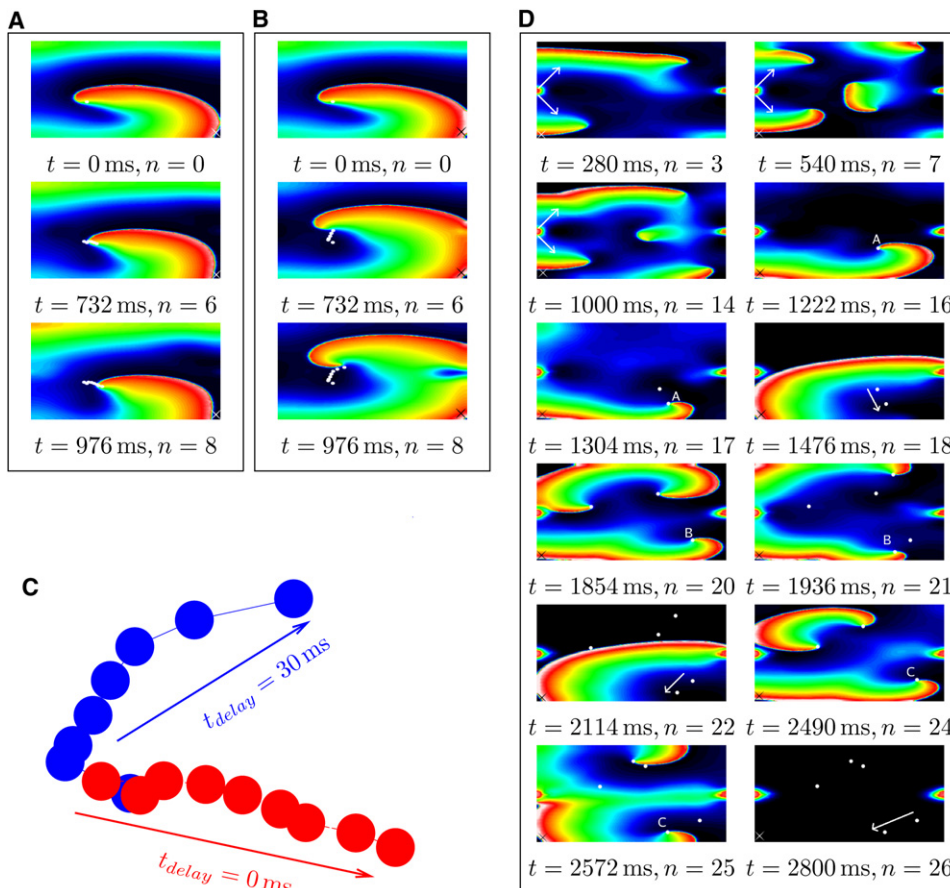
FIGURE 7 Resonant drift of a meandering pattern with (A) $t_{delay} = 0$ ms and (B) $t_{delay} = 30$ ms; $A = 1 \times 10^6 \, \mu A/cm^3$. (C) Tip trajectories of patterns A and B enlarged. (D) Effect of increasing t_{delay} to 30 ms at $t = 1000$ ms to the infinite loop shown in Fig. 6 A: the reentry is extinguished. (Arrows) Generation of new waves and the direction of drift. (NB, resonant drift pacing handles multiple patterns.)

(21). Here we have demonstrated that the far-field action of the electric current can cause, under repetitive stimulation, a drift and elimination of the reentrant sources. In our simulations, resonant drift pacing can eliminate reentry, including multiple reentries, with high probability and within acceptable time, at amplitudes much lower than single-shock defibrillation. If we allow 10 s for low-voltage reentry termination, as is the case for antitachycardia pacing, the required shock strength with resonant drift pacing is 12–15 times smaller than with a single shock.

Our simulations have shown that a major possible obstacle to elimination of reentrant sources is the possibility that the electric shocks create new reentrant waves while eliminating existing ones, which could possibly lead to infinite loops of annihilation and creation. The creation of the new sources occurs near the shock electrodes where the electric field is highly inhomogeneous, and the 12–15-fold decrease in defibrillation threshold is observed, notwithstanding this effect. The highly inhomogeneous electric field is created by point electrodes; therefore, bigger electrodes, which create fields that are more homogeneous, should perform even better.

Our simulations have also demonstrated yet another way to overcome infinite annihilation-creation loops. This is due to the dependence of the direction of resonant drift on the time delay in the feedback loop. This dependence has been predicted and observed in isotropic monodomain models with simplified description of the electric field action (15,17,19,25,32). Here we demonstrated that this dependence is still observed in this more realistic model and, moreover, it can be used to discontinue an infinite annihilation-creation loop, via a change in the feedback delay once such a loop has been detected.

Although we used atrial tissue kinetics, there are indications that the exact sort of excitable kinetics is not too important for the properties of resonant drift (19,25). We therefore expect that these results could be interesting for ventricular fibrillation as well.

Comparison with previous research

Antitachycardia pacing

In clinical practice, antitachycardia pacing is as efficient and safe as single-shock defibrillation, even for fast ventricular tachycardias with up to 250 beats/min (14). The exact mechanisms underlying the success or failure of antitachycardia pacing are, for the most part, unexplored. The traditional understanding implies stimulation that is faster than the anatomical reentry and that engages an ever increasing area of tissue until it reaches an isthmus of the reentry and blocks it. It is conceivable, however, that in some cases antitachycardia pacing may be unwittingly applied to a functional

rather than anatomical reentry and then its mechanism could be the resonant drift. In such cases, feedback-controlled resonant drift pacing will do a better job than the pacing with prescribed frequency used in antitachycardia pacing. Although the probability of antitachycardia pacing success is high, when it fails, a single strong shock has to be applied.

Unpinning

It has been speculated that anatomically or functionally anchored ventricular tachycardias are less likely to be terminated by antitachycardia pacing. For these cases, it has been suggested that a weak shock, with an amplitude in the range used in this study, can be applied to unpin the reentry from the obstacle by a virtual electrode polarization mechanism (33,34). Such a stimulus must be correctly timed, which can be achieved by synchronizing it to the signal from a registration electrode, with a correctly chosen delay with respect to that signal, which in practice may require scanning through possible delays. The resonant drift pacing also requires synchronization with a registered signal, and we have seen that change in the delay during the course of pacing may also be beneficial. This makes the unpinning protocol operationally very similar to our resonant drift pacing protocol, and in any particular case it may not be possible to say with certainty which mechanism has worked.

Experiments with feedback-controlled pacing

Pak et al. (31) eliminated ventricular fibrillation in rabbit by multisite pacing synchronized with optical signal from a fixed reference site. Their stimulation protocol was similar to resonant drift pacing considered here, except they used more pacing electrodes and aimed to deliver shocks only when pacing site was in an excitable gap, under the implicit assumption that shock delivered to a site in an absolute refractory state could not possibly affect the reentry, i.e., a priori ignoring far-field effects. Despite this artificial self-limitation, they were successful at defibrillating with shock strengths one-order-of-magnitude lower than single-shock defibrillation and with better success rate than overdrive and high-frequency pacing. It was argued in Pak et al. (31) that earlier mathematical modeling of resonant drift only demonstrated termination of a single reentrant wave (see, however, (32)) and their experiments did not show evidence of extinction of reentries on ventricular borders. Our present simulations indicate that

  Far-field effects can make it worthwhile issuing shocks regardless of the tissue state at the pacing site.

  The resonant drift pacing can work for multiple reentrant waves (providing that the difficulties of new wavefronts being initiated by the shocks are overcome).

  Annihilation at the boundaries is not a necessary feature of resonant drift elimination, as reentry sources can annihilate with each other.

Thus, we find the results by Pak et al., contrary to their own interpretation, to be strong experimental evidence of the resonant drift pacing being an efficient method of low voltage defibrillation.

Clinical implications

Resonant drift pacing may present an alternative or a supplement for existing therapies (single-shock defibrillation, synchronized cardioversion, antitachycardia pacing, overdrive pacing, and high-frequency pacing) and the one proposed (unpinning). The theoretical mechanism underlying this protocol is for functionally determined reentries, i.e., probably for higher frequency tachycardias and fibrillations. Due to similarity between resonant drift and unpinning pacing protocols, the two protocols may be possible to combine into one, which would work via unpinning for pinned (monomorphic tachycardias), and via resonant drift for unpinned reentrant waves (polymorphic tachycardias and fibrillations).

There is evidence that some atrial arrhythmias are not reentrant, but are due to rapid ectopic focal activity (35). The proposed method might work on such arrhythmias via a completely different mechanism, say overdrive suppression, but this can only be clear after further studies.

As this study is purely theoretical, the key question is whether the low-energy approach to defibrillation considered here could work in a real heart. Clearly this question can only be answered by experimental studies.

Study limitations

Apart from inevitable limitations inherent in mathematical modeling compared to experimental study, which are due to limited current knowledge, we have made a number of simplifications. Our model tissue was essentially two- rather than three-dimensional. Its geometry was not realistic (rectangular shape). The model tissue lacked any macroscopic inhomogeneities, such as transmural, center-periphery or base-apex gradient of excitability properties, or variations of the conductivity tensor. The position and geometry of the electrodes was arbitrary. Values of some of the parameters lack reliable experimental foundation, including some of the most important ones, such as F, the intracellular conductivity fluctuations amplitude. The spatially uncorrelated structure of conductivity fluctuations is an idealization. These limitations can be lifted as more experimental data become available and via further, more detailed, simulation studies.

Resonant drift pacing may potentially work for ventricular tachycardia and fibrillation as well. However, the ventricles have thick walls and overall more complicated anatomy, which may pose extra difficulties for defibrillation. So any extrapolation of our present results to ventricles should be considered with caution, bearing in mind possible complications. There are modeling studies suggesting that at least some of the new difficulties arising in resonant pacing of three-dimensional reentries can be successfully overcome

(see (36) and references therein); however, those were in overly simplified models of excitable media, and more realistic computational studies are still desirable.

CONCLUSION

Our results show that in a bidomain model of cardiac tissue, with microscopic conductivity fluctuations, reentrant waves can be annihilated using feedback-controlled repetitive stimulations by inducing resonant drift and directing the reentry toward an inexcitable boundary. If associated difficulties are overcome, termination using this approach is achieved, with high probability and within acceptable time, at a fraction of the conventional shock strength. The direction of the drift can be managed by choosing the location of the electrodes and the time delay of the shock application.

Difficulties occur due to new wavefronts being initiated from the shock electrodes. However, numerical simulations allow a detailed insight into this problem and can be used as a tool to suggest solutions.

Our findings present experimentally testable hypotheses for what we expect to observe in real cardiac tissue. There is scope for advance in the field of low-energy defibrillation, by interaction between modeling studies such as this one, and experimental studies.

SUPPORTING MATERIAL

Movies and their legends are available at http://www.biophysj.org/biophysj/supplemental/S0006-3495(09)00012-5.

REFERENCES

1. Lee, D. S., L. D. Green, P. P. Liu, P. Dorian, D. M. Newman, et al. 2003. Effectiveness of implantable defibrillators for preventing arrhythmic events and death: a meta-analysis. *J. Am. Coll. Cardiol.* 41:1573–1582.

2. Malkin, R. A. 2002. Large sample test of defibrillation waveform sensitivity. *J. Cardiovasc. Electrophysiol.* 13:361–370.

3. DeBruin, K. A., and W. Krassowska. 1999. Modeling electroporation in a single cell. I. Effects of field strength and rest potential. *Biophys. J.* 77:1213–1224.

4. Sambelashvili, A. T., V. P. Nikolski, and I. R. Efimov. 2004. Virtual electrode theory explains pacing threshold increase caused by cardiac tissue damage. *Am. J. Physiol. Heart Circ. Physiol.* 286:H2183–H2194.

5. Sharma, V., R. C. Susil, and L. Tung. 2005. Paradoxical loss of excitation with high intensity pulses during electric field stimulation of single cardiac cells. *Biophys. J.* 88:3038–3049.

6. Zivin, A., J. Souza, F. Pelosi, M. Flemming, B. P. Knight, et al. 1999. Relationship between shock energy and postdefibrillation ventricular arrhythmias in patients with implantable defibrillators. *J. Cardiovasc. Electrophysiol.* 10:370–377.

7. Kamm, R. M., H. Garan, B. A. McGovern, J. N. Ruskin, and J. W. Harthorne. 1997. Transient right bundle branch block causing R wave attenuation postdefibrillation. *Pacing Clin. Electrophysiol.* 20:130–131.

8. Tokano, T., D. Bach, J. Chang, J. Davis, J. J. Souza, et al. 1998. Effect of ventricular shock strength on cardiac hemodynamics. *J. Cardiovasc. Electrophysiol.* 9:791–797.

9. Boriani, G., M. Biffi, P. Silvestri, C. Martignani, C. Valzania, et al. 2005. Mechanisms of pain associated with internal defibrillation shocks: results of a randomized study of shock waveform. *Heart Rhythm.* 2:708–713.

10. Jung, J., A. Heisel, R. Fries, and V. Kollner. 1997. Tolerability of internal low-energy shock strengths currently needed for endocardial atrial cardioversion—effect on atrial defibrillation threshold and pain perception. *Am. J. Cardiol.* 80:1489–1490.

11. Walcott, G. P., R. G. Walker, A. W. Cates, W. Krassowska, W. M. Smith, et al. 1995. Choosing the optimal monophasic and biphasic waveforms for ventricular defibrillation. *J. Cardiovasc. Electrophysiol.* 6:737–750.

12. Zhang, Y., B. Rhee, L. R. Davies, M. B. Zimmerman, D. Snyder, et al. 2006. Quadriphasic waveforms are superior to triphasic waveforms for transthoracic defibrillation in a cardiac arrest swine model with high impedance. *Resuscitation.* 68:251–258.

13. Sullivan, J. L., S. B. Melnick, F. W. Chapman, and G. P. Walcott. 2007. Porcine defibrillation thresholds with chopped biphasic truncated exponential waveforms. *Resuscitation.* 74:325–331.

14. Wathen, M. S., P. J. DeGroot, M. O. Sweeney, A. J. Stark, M. F. Otterness, et al. 2004. Prospective randomized multicenter trial of empirical antitachycardia pacing versus shocks for spontaneous rapid ventricular tachycardia in patients with implantable cardioverter-defibrillators: pacing fast ventricular tachycardia reduces shock therapies (PainFREE Rx II) trial results. *Circulation.* 110:2591–2596.

15. Davydov, V. A., V. S. Zykov, A. S. Mikhailov, and P. K. Brazhnik. 1988. Drift and resonance of spiral waves in active media. *Radiofizika.* 31:574–582.

16. Agladze, K. I., V. A. Davydov, and A. S. Mikhailov. 1987. An observation of resonance of spiral waves in distributed excitable medium. *JETP Lett.* 45:767–770.

17. Biktashev, V. N., and A. V. Holden. 1994. Design principles of a low voltage cardiac defibrillator based on the effect of feedback resonant drift. *J. Theor. Biol.* 169:101–112.

18. Zykov, V. S., and H. Engel. 2007. Analysis and Control of Complex Nonlinear Processes in Physics, Chemistry and Biology, Vol. 5. World Scientific Lecture Notes in Complex Systems, World Scientific, Singapore.

19. Biktashev, V. N., and A. V. Holden. 1996. Reentrant activity and its control in a model of mammalian ventricular tissue. *Proc. R. Soc. Lond. B. Biol. Sci.* 263:1373–1382.

20. Panfilov, A. V., S. C. Muller, V. S. Zykov, and J. P. Keener. 2000. Elimination of spiral waves in cardiac tissue by multiple electrical shocks. *Phys. Rev. E Stat. Phys. Plasmas Fluids Relat. Interdiscip. Topics.* 61:4644–4647.

21. Plank, G., L. J. Leon, S. Kimber, and E. J. Vigmond. 2005. Defibrillation depends on conductivity fluctuations and the degree of disorganization in reentry patterns. *J. Cardiovasc. Electrophysiol.* 16:205–216.

22. Trayanova, N. 2006. Defibrillation of the heart: insights into mechanisms from modeling studies. *Exp. Physiol.* 91:323–337.

23. Potse, M., B. Dube, J. Richer, J. Vinet, and R. M. Gulrajani. 2006. A comparison of monodomain and bidomain reaction-diffusion models for action potential propagation in the human heart. *IEEE Trans. Biomed. Eng.* 53:2425–2435.

24. Courtemanche, M., R. J. Ramirez, and S. Nattel. 1998. Ionic mechanisms underlying human atrial action potential properties: insights from a mathematical model. *Am. J. Physiol.* 275:H301–H321.

25. Biktashev, V. N., and A. V. Holden. 1995. Control of reentrant activity in a model of mammalian atrial tissue. *Proc. R. Soc. Lond. B. Biol. Sci.* 260:211–217.

26. Vigmond, E. J., and G. Plank. Cardiac Arrhythmia Research Package (CARP). http://carp.meduni-graz.at.

27. Vigmond, E. J., M. Hughes, G. Plank, and L. J. Leon. 2003. Computational tools for modeling electrical activity in cardiac tissue. *J. Elec.* 36(Supp.):69–74.

28. Plank, G., M. Liebmann, R. Weber dos Santos, E. J. Vigmond, and G. Haase. 2007. Algebraic multigrid preconditioner for the cardiac bidomain model. *IEEE Trans. Biomed. Eng.* 54:585–596.

29. Kneller, J., R. Zou, E. Vigmond, Z. Wang, L. J. Leon, et al. 2002. Cholinergic atrial fibrillation in a computer model of a two-dimensional sheet of canine atrial cells with realistic ionic properties. *Circ. Res.* 90:E73–E87.

30. Xie, F., Z. Qu, A. Garfinkel, and J. N. Weiss. 2002. Electrical refractory period restitution and spiral wave reentry in simulated cardiac tissue. *Am. J. Physiol. Circ. Physiol.* 283:448–460.

31. Pak, H., Y. Liu, H. Hayashi, Y. Okuyama, P. S. Chen, et al. 2003. Synchronization of ventricular fibrillation with real-time feedback pacing: implication to low-energy defibrillation. *Am. J. Physiol. Heart Circ. Physiol.* 285:H2704–H2711.

32. Biktashev, V. N., and A. V. Holden. 1995. Resonant drift of autowave vortices in two dimensions and the effects of boundaries and inhomogeneities. *Chaos Solitons Fractals.* 5:575–622.

33. Ripplinger, C. M., V. I. Krinsky, V. P. Nikolski, and I. R. Efimov. 2006. Mechanisms of unpinning and termination of ventricular tachycardia. *Am. J. Physiol. Heart Circ. Physiol.* 291:H184–H192.

34. Cysyk, J., and L. Tung. 2008. Electric field perturbations of spiral waves attached to millimeter-size obstacles. *Biophys. J.* 94:1533–1541.

35. Nattel, S. 2002. New ideas about atrial fibrillation 50 years on. *Nature.* 415:219–226.

36. Morgan, S. W., I. V. Biktasheva, and V. N. Biktashev. 2008. Control of scroll-wave turbulence using resonant perturbations. *Phys. Rev. E Stat. Nonlin. Soft Matter Phys.* 78:046207.